Additive Manufacturing Letters 17 (2026) 100354

Contents lists available at ScienceDirect

Additive Manufacturing Letters

journal homepage: www.elsevier.com/locate/addlet

Short Communication

Approximation of absorptivity conditions for Inconel 625 from in situ radiation thermometry measurements in electron beam powder bed fusion

Shadman Tahsin Nabil [a,b], Alfonso Fernandez [d], Francisco Medina [a,b], Ralph Felice [c], James P. Carney [a,b], César A. Terrazas-Nájera [a,b,*]

[a] Department of Aerospace and Mechanical Engineering, The University of Texas at El Paso, El Paso, TX, 79968, USA
[b] W. M. Keck Center for 3D Innovation, Advanced Manufacturing and Aerospace Center, The University of Texas at El Paso, 500 W. University Ave., El Paso, TX, 79968, USA
[c] FAR Associates, Macedonia, OH, 44056, USA
[d] Sandia National Laboratories, Center for Advanced Manufacturing Innovation, NM, 87123, USA

ARTICLE INFO

Keywords:
Absorptivity
Temperature
Powder bed fusion
Spectral
Nickel-base alloys
Energy balance

ABSTRACT

Highly dynamic conditions experienced during metals processing using powder bed fusion (PBF) additive manufacturing (AM) arise from the interaction of multiple process variables. Chiefly amongst them is the energy source-material interaction, which results in abrupt, temporally changing thermal conditions at the melt-pool. The absorption of the energy from the source by the powder bed is complicated complex because this interaction is highly dynamic and occluded by process emissions including the plasma plume and spatter. Typical approaches for measuring absorption conditions have relied on intricate *ex situ* setups requiring extensive sample preparation. This work involved approximating the absorptivity for a nickel-base material from in situ observations made using a multi-wavelength (MW) pyrometry sensor, while processing using electron-beam based powder bed fusion (PBF-EB/M). The prediction step involved fitting the spectral data captured by the MW sensor to then extrapolate values to shorter wavelengths. The approximation was done for wavelengths that are relevant for the PBF-LB/M process, where absorptivity of the laser energy is paramount. The results obtained provide a window into the behavior of this material as it transitions from powder to molten state, showing that the absorptivity substantially decreases (~60% reduction) as the powder material changes phase induced by incipient melting. While this work focuses on a single material, the approach presented can help characterize the absorptivity of other materials employed in PBF. This work helps support both experimental and modeling efforts that are helpful to increase our understanding and practice of fusion-based AM processes, and other manufacturing techniques.

Introduction

The thermal history plays an important role in any manufacturing involving phase transitions of matter. This is specifically relevant during powder bed fusion (PBF) additive manufacturing (AM) where the layer-by-layer fabrication induces continued thermal cycling of the material. Nevertheless, unlike conventional manufacturing, where the entire heating and cooling processing typically occurs in bulk, during fusion-based AM process the transitions that take place are highly localized since the energy source is scanned to achieve selective melting. This results in the development of a melt-pool –the interaction zone of the source with the material– transitioning through multiple phases (powder, liquid, and solidified material, or a mixture of these), each having distinct thermal radiative properties such as emissivity and absorptivity.

Under conditions of incident energy irradiation on a given material the thermal radiative behavior is characterized by its absorptivity (α), reflectivity (ρ) and transmissivity (τ). These optical radiative properties describe the energy absorbed, reflected and transmitted from the surface of the irradiated material adding to unity under a set of observation conditions defined spectrally and thermally. For opaque materials, only absorptivity and reflectivity remain since the transmissivity is considered zero.

For the laser-based powder bed fusion (PBF-LB/M) additive

* Corresponding author.
E-mail address: caterrazas2@utep.edu (C.A. Terrazas-Nájera).

https://doi.org/10.1016/j.addlet.2026.100354
Received 7 October 2025; Received in revised form 7 December 2025; Accepted 5 January 2026
Available online 6 January 2026

manufacturing (AM), absorption of the energy from the laser is critical during processing; the efficiency with which the laser energy is absorbed by the material directly influences the laser-material interactions and hence the stability of the process, ultimately impacting the mechanical performance of the built components. Typically, for a given material, the laser energy must be tuned within a controlled process parameter window to remain in conduction, transition, or keyhole modes, and prevent the development of defects, including lack of fusion and porosity. While the process appears cleaner in the conduction mode, the stable keyhole mode is preferred as it allows for penetration into previously deposited layers, enhancing bonding and preventing issues such as delamination and lack of fusion [1]. However, processing under an unstable keyhole mode can lead to increased porosity creation and spatter ejection after the development of the well-studied keyhole effect [2–4].

Further, the absorption conditions are intrinsically linked to the scanning conditions; although not traditionally considered, the laser-material interactions are necessarily controlled by the absorptivity of the powder bed material, which evolves along with the dynamics of the PBF-LB/M process as the material is subjected to phase changes driven by the interaction of the energy source and the rest of the thermal environment [3,4].

The most common energy source employed in PBF-LB/M AM is a high-brightness monochromatic infrared (IR) laser having a typical Gaussian distribution (TEM00 mode). The reduced absorption of IR laser energy when processing materials with high reflectivity including pure copper and copper alloys has nevertheless been a challenge [5,6]. Recently, lasers emitting within the visible spectrum (lower than IR) have been proposed for addressing this challenge; laser frequencies that include green (typically at 532 nm or 515 nm) and blue (450 nm) have been reported [7–11]. The widespread applicability of these laser sources is hindered by an increased initial capital investment, as well as higher operating costs for green lasers, and the reduced brightness and control of the energy delivery through scanning devices at the required focus spot sizes for blue lasers [7]. Despite this, it appears IR lasers will remain as the preferred laser source for metals PBF-LB/M, as exemplified by recent developments such as beam shaping of the intensity profile [12–14], and the trend towards increased wattage of IR lasers that help overcome the reduced absorptivity issues experienced with highly reflective materials [15–17].

In-process measurements during PBF-LB/M are challenging given the various process effects including the plasma plume, spatter, and the denudation around the melt pool than can bias the obtained results [18–21]. The capture of process signatures to obtain thermal radiative properties such as absorptivity is subjected to the same process occlusions which has led the community to resort to the use of constant values for properties such as emissivity and absorptivity [22], or employ proxy measurements performed *ex situ*, for samples that have been extensively prepared. These experiments are typically done employing elaborate calorimetry or optical setups such as integrating spheres, using conditions that approximate PBF-LB/M such as single line scans on bare metal plates [5,23–25]. Integrating spheres are suitable devices for measurement of optical radiative properties such as reflectance and absorptance but their drawback is the inability to be used at elevated temperatures such as those observed during PBF AM [26]. Also, absorption effects within the coatings used in integrating spheres can skew the results obtained [27]. Simonds *et al.* compared the integrating sphere and the calorimetry methods and found the latter measures substantially less energy absorbed compared to the former [28]. Nevertheless, the ability to capture in-process emissions from which thermal radiative behavior or character can be established is actively being researched. For example, Trapp *et al.* carried out absorptivity measurements in situ for metallic powders employing a micro-calorimetry apparatus within a PBF system [29]. While this work presented data captured under conditions similar to those observed during the actual processing, the setup relied on single track scans, which might not fully represent a multi-layer build typical of the PBF-LB/M process. As identified by Rubenchick *et al.* [27], there is a need for pedigree data detailing the temperature dependence of absorptivity and in general of in situ absorptivity measurements. This knowledge can serve to inform experimental and modeling efforts aimed at increasing our understanding of the PBF process and in furthering the industrial adoption of PBF AM [30].

Recent works from our group employing a multi-wavelength (MW) pyrometry technique have shown the highly variable thermal emissive behavior both spectrally and temporally for materials during in-process conditions using electron beam-based powder bed fusion (PBF-EB/M), specifically in various phases of interest including powder, molten or liquid, and solidified material [31,32]. The MW technique employed in these prior works can provide emissivity-independent accurate temperatures and, using Planck's distribution equation, a back calculated measure of the emissive power (emissivity or signal strength) of the target observed in a calibrated spectral range from spanning from 1080 - 1637 nm [33]. Building upon these prior works, the following describes the application of energy balance to approximate the absorptivity conditions for an Inconel 625 material processed via PBF-EB/M [31]. In the current work, spectral data that was collected during PBF-EB/M processing of Inconel 625 was employed along with energy balance, to approximate the absorptivity conditions for the material at relevant process temperatures, and at frequencies of interest for PBF-LB/M.

The results presented in this work detail a decrease in the absorptivity for Inconel 625 from ~0.6 in the heated powder condition, to below ~0.2 as the material transitions into the molten or liquid state. While the measurements that will be presented in this work were done in the PBF-EB/M process, they can be applicable to PBF-LB/M because the exhibited thermal radiative behavior or character is independent of the irradiating source. The MW pyrometry technique resolves the emissivity spectrally within the calibrated range using the optics of the device [34], and by energy balance, the absorptivity can be inferred. Also, as discussed in our prior works [31,35], the use of PBF-EB/M provide a pristine environment (i.e. vacuum), allowing for gathering spectral data at temperatures of interest (> 400 °C), and substantially reducing the process occlusions including plasma and high spatter that are typical of PBF-LB/M. The oxidation of samples, which is a common occurrence in other *ex situ* setups including integrating sphere reflectometer techniques, was also prevented by employing the PBF-EB/M platform. Finally, the irradiation using the electron beam eliminated the susceptibility for oversaturation of the sensors employed by the MW pyrometer at the IR frequencies typical of the lasers used in the PBF-LB/M process, which could have biased the temperature, tolerance, and signal strength calculations. Nevertheless, it is acknowledged that measurements from the PBF-LB/M process are required to consider specific process effects that occur in this process, that might lead to differences in the behavior of absorptivity measured and estimated here using PBF-EB/M, particularly during the development of keyholing, where absorptivity might locally increase, as shown recently in [36]. This is the subject of ongoing research.

Methodology

Experimental

The experimental setup employed [31] involved a commercial GE-Arcam A2X (GE Additive, US) PBF-EB/M system that was used to deposit a cylindrical part –serving as the target for observation and measurements– along with other multiple adjacent but separate rectangular prismatic parts in an Inconel 625 powder bed. The dimensions of the target were 8 mm in diameter and 10 mm in height. The Inconel 625 powder utilized for experiments had a particle size distribution from 45–106μm, d50 of 70μm (Praxair, USA). Specifics of the Inconel 625 feedstock are presented in greater detail in [32]. The surface of the target was tracked by employing an FMPI multi-wavelength pyrometer (FAR Associates, OH, USA) that was used with a custom optical design that prevented metallization of the glass elements in the optical path and

hence enabled continuous measurements through the various phase transitions experienced by the material as described previously by [35]. For this work, the monitored region of the target comprised a ~2.7 mm diameter spot. Also, a radiometric calibration was done for the FMPI using a conical IR-563 blackbody source (Infrared Systems Development, FL, USA) to a stabilized temperature of 1000 °C.

The FMPI captures the brightness or intensity values of a measured target that are subsequently corrected through the radiometric calibration. Then, a mathematical approximation of Planck's distribution is produced which is used to calculate a matrix of temperatures from wavelength-intensity pairs. Next, the device performs some checks for consensus and corrections for the spectral intensity dependence (if detected). Finally, it computes the consensus temperature, the tolerance (a measure of the temperature accuracy), and the signal strength (the spectral emissivity modified by the optical environment). The FMPI was used with its factory settings for exposure time spanning from 4μs to 8s. Each measurement is reported in a log file with a corresponding file with the spectral data also stored. The spectral data captured was employed in this research to predict values for the signal strength at the 1064–1070 nm wavelength range.

For the results to be presented in this work, the dataset consisted of measurements made during an experiment observing continuous deposition of several layers that underwent fresh powder recoating, preheating and melting of the Inconel 625 powder. The data was categorized by phase (preheating, melt scanning or cooldown), which allowed to observe the transitions from incipient melting into the liquid (molten) phase for several layers monitored. The data collected in this experiment involved the aggregated data for 18 consecutive layers. This aggregation of the data revealed the pattern or trend of the signal strength or emissivity during the melting excursions.

Mathematical formulation

Thermal radiation is emitted by matter above absolute zero ($T > 0$ K) having internal energy arising from atomic movement and interactions. Temperature is an indicator of this internal energy of matter, which can be related to the brightness or intensity emitted. Planck's distribution law solved for the two-color pyrometry (Eq. (1)) and its solution for emissivity (Eq. (2)) are employed by the FMPI to compute the temperature and signal strength (emissivity) from the brightness measured for the target.

$$T_{1,2} = \frac{C'\left(\frac{1}{\lambda_2} - \frac{1}{\lambda_1}\right)}{lnR - 5\ln\left(\lambda_2/\lambda_1\right)} \tag{1}$$

$$\varepsilon_{(\lambda)} = \frac{L\lambda^5\left[e^{hc/\lambda k_B T} - 1\right]}{2hc^2} \tag{2}$$

In Eq. (1), C' represents the second radiation constant, the λ terms are the two wavelengths (channels) chosen and R is the ratio of the brightness or intensities (I_2/I_1) measured at λ_1 and λ_2. For each measurement, the FMPI utilizes a process that effectively generates a multitude of virtual 2-color pyrometers each calculating a temperature that is later used to compute the consensus or final temperature reported [37] as detailed above. For Eq. (2), h is Planck's constant, L is the radiation quantified, λ is the wavelength, ε the emissivity, c is the speed of light, and K_B is Boltzmann's constant.

Although process conditions are generally considered far-from-equilibrium for PBF AM, arguments can be made to support the assumption of local thermal equilibrium for the target being measured in this work; first, the target is surrounded by metal powder on its sides providing a high degree of thermal insulation. Also, whereas the previously deposited and solidified metal provides a thermal conduction path, the validity of the thermal equilibrium is still applicable as the whole fabrication substrate sits on a powder bed which remains at elevated temperature throughout the fabrication process via preheating using scanning of the electron beam. Second, the exposed surface is in vacuum with a limited radiation interaction within the processing chamber; as shown by Fernandez *et al.,* the enclosure temperatures in the Arcam A2X remain well below the threshold where they can have a meaningful impact or interaction with the target and hence the measurements of the MW pyrometer sensor [35]. Of particular interest is the data showing the transition from powder to liquid, as this is the regime where the absorption conditions are changing the most and have a direct effect on the processing and quality during metal deposition. Under this premise of thermal equilibrium and by energy balance, the absorptivity was approximated for the material in the phase change regime from incipient melting (i.e. scanning with the beam) and into the liquid or molten phase. This was done by invoking Kirchoff's law of thermal radiation (Eq. (3)) which provides the equivalence of emissivity (ε) to absorptivity (α) for a given set of spectral and thermal conditions, as indicated in Eq. (3), with subscripts indicating the spectral (λ), and thermal (T) dependencies:

$$\varepsilon_{\lambda,T} = \alpha_{\lambda,T} \tag{3}$$

Spectral data

The FMPI captures the intensity or brightness (L) of the target through its entire detector range but only reports calibrated spectral data for every measurement in the range from 1080–1637 nm, by separating the intensity or brightness observed through an optical grating. Nevertheless, the absorptivity data is of interest at the infrared (1064–1070 nm) frequencies typically employed by PBF-LB/M systems. To extrapolate to frequencies of interest, the spectral data for each measurement made was analyzed and used to predict the values of emissivity at these IR laser frequencies. This involved a polynomial regression fit followed by calculation of the 95 % confidence interval, and then the calculation, using the polynomial equation, of values expected in the 1064 to 1070 nm range. For the regression fit, the data falling within the water absorption region 1315–1455 nm (indicated as a light blue box) was disregarded but is shown in plots in the results, for clarity.

Results

Temperature

Using the setup described in the experimental section, the FMPI was used to capture measurements during the deposition of consecutive layers. Fig. 1 shows the plot of temperature (in degrees °C) versus time (seconds) for the entire duration of the experiment. In this figure, horizontal lines indicate the range of temperatures for which Inconel 625 undergoes incipient melting (1290–1350 °C). In this plot, the data shows relatively consistent behavior for measurements in each layer with slight differences in the maximum temperatures measured given variations in the direction of the scanning strategy, leading to potentially missing measurement of certain values, as was detailed in [35]. Nevertheless, the chart shows that the melting range (semitransparent orange region) is reached for all layers monitored. Also, as shown in Fig. 1B) the preheat phase is characterized by two sub-phases, one of them with values that oscillate in an approximate range from ~930 to ~1050 °C and spans for about 5 s while the second sub-phase raises temperature in the range from ~960 to 1085 °C and lasts ~7 s.

Emissive behavior during melting

The aggregated data for 18 layers during melting excursions (i.e. scanning leading to increases in temperature within the melting range) is shown on Fig. 2 for the median calibrated wavelength value of 1500 nm. The melting range is indicated by a semitransparent orange box and limits as vertical lines with temperature values.

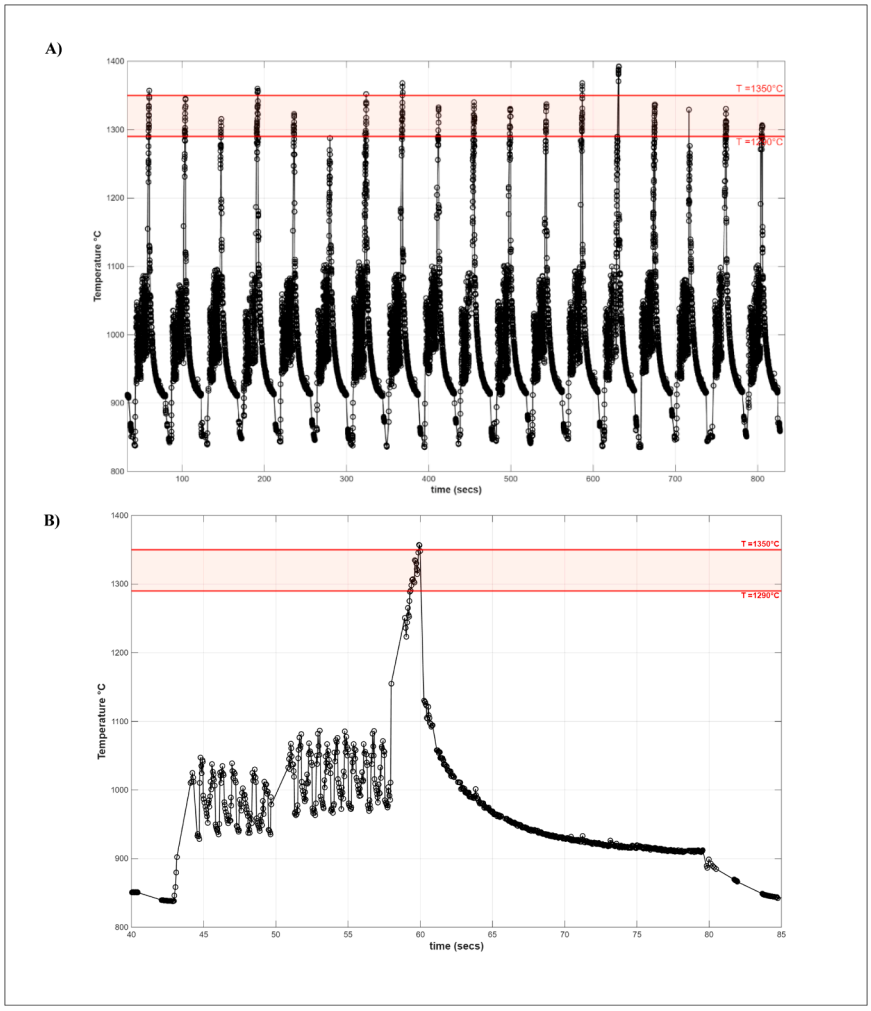

Fig. 1. A) Temperature as a function of time (seconds) showing the total layers monitored, and B) profile of temperature vs time for a single layer.

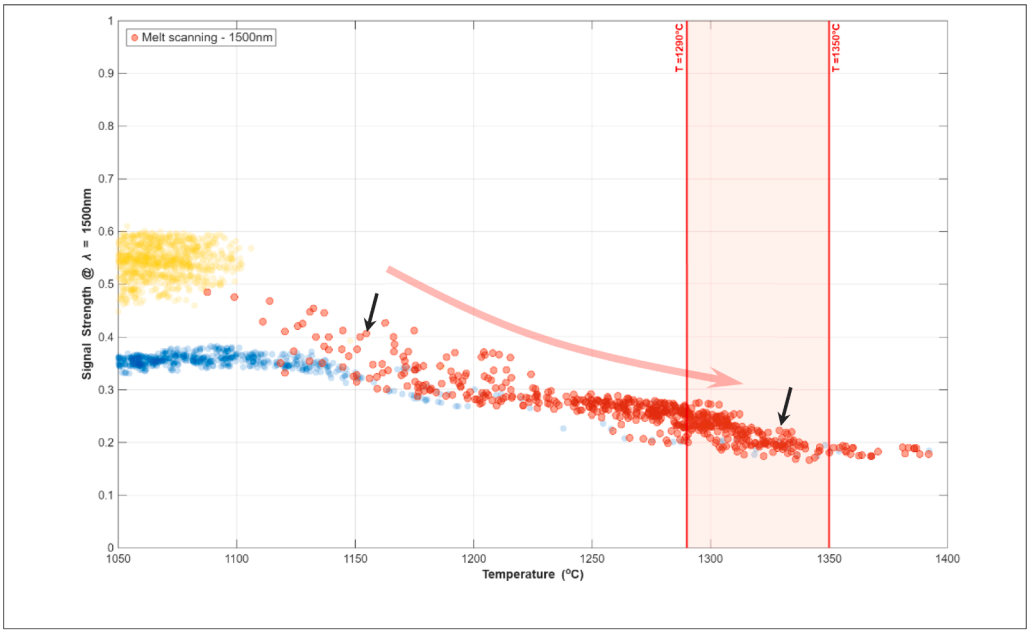

Fig. 2. Signal strength (@ 1500 nm) versus Temperature showing melt scan excursions. Aggregated data for 18 layers. Color of markers indicates phase: preheat (yellow), melt scanning (red), cooldown (blue).

In Fig. 2, the preheat and cooldown regions are shown with faded color (yellow and blue, respectively) while measurements in the melt scanning region are prominently shown with red circle markers for emphasis, as this is the phase transition of primary interest for this work and in general for understanding absorptivity conditions in PBF AM. For context, during the melt excursions, the data observes a trend of increasing temperature (from maximum values attained during pre-heating at ~1185 °C, to values well within or exceeding the melting range) with a corresponding decrease in signal strength, from average values ~0.6 at the beginning of the melt scanning to <0.2 at the molten state. In this figure, the occurrence and trend of the melting excursions are emphasized by the faded red arrow.

Absorptivity approximation

Following the process detailed in the methods section above, the fitting of the spectral data (in the 1080–1637 nm range) was done for each datapoint that was assigned to the melt scanning phase (red datapoints in Fig. 2). Then, expected or predicted values in the range from 1064–1070 nm were computed using the fitted equation. Fig. 3 shows the fit analysis and calculation of the predicted values for two data points of interest indicated by dark arrows in Fig. 2. These plots in Fig. 3 show the spectral data captured by the FMPI for a single datapoint with the fitted polynomial (red solid line) and 95 % CI limits (dashed black lines). Then, the extrapolated values within the range from 1064 - 1070 nm are shown as green asterisks. As has been discussed previously,

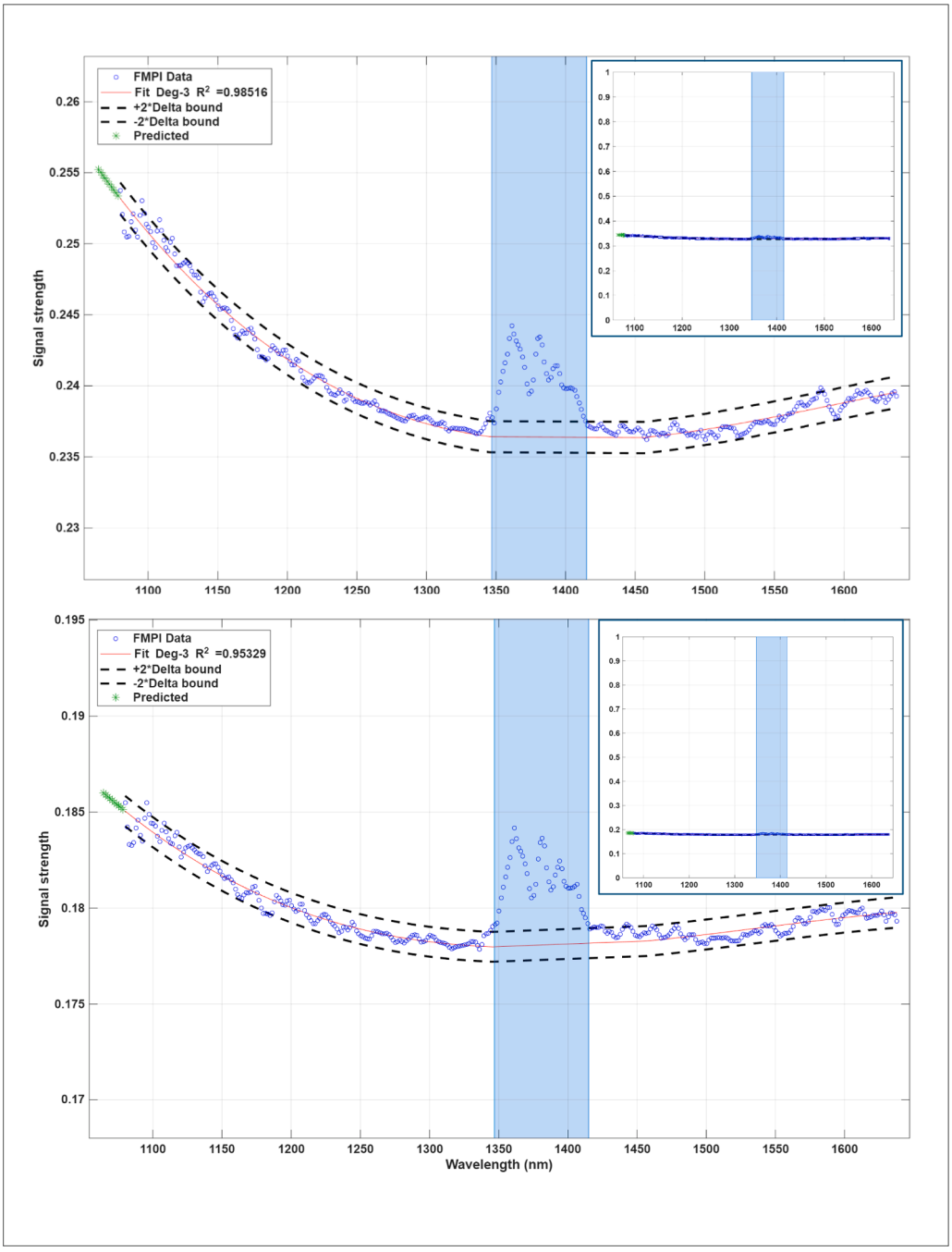

Fig. 3. Spectral data analysis for datapoints of interest selected in Fig. 2. Note that increasing the limits from 0 to 1 for the y-axis, shows the linearity (gray behavior) of spectral data (insets).

the values were predicted in the wavelength range from 1064–1070 nm as these are the typical frequencies employed by near IR lasers that are the most commonly used source for the PBF-LB/M process.

Once the spectral calculations were done for each datapoint identified in the melt scanning phase, the back calculated signal strength versus temperature plot was obtained for wavelengths of 1064 nm and 1070 nm. Fig. 4 shows the comparison (superimposed datasets) of signal strength measurements reported by the FMPI at 1500 nm (red circles), versus the calculated values for emissivity (or by equivalence absorptivity) at 1064 nm (green squares), and 1070 nm (light blue diamonds). Alpha or transparency values for the markers in the plot were set to 50 % to enhance visibility.

Discussion

The data in Fig. 4 shows that there is minor variability when comparing the measured values for the signal strength at the reported wavelength of 1500 nm and those predicted by our approach for shorter wavelengths of 1064 nm and 1070 nm. Although the extrapolated signal strength values (i.e. 1070 nm and 1064 nm) are slightly higher than measured values at 1500 nm obtained from the pyrometer, such declining trend is consistent with the general observation that as the wavelength increases, the emissivity for metals typically exhibits a monotonically decreasing trend, as detailed in the Thermal Radiative Properties (TPRC) compendium [38] and observed for our data in Fig. 3. This decreasing behavior is not directly appreciable in Fig. 4, but it is more apparent in the spectral plots in Fig. 3 with the values declining from short to long wavelengths (i.e. overall decreasing trend but more specifically from 1100 nm to 1300 nm). It is also instructive to mention that while the behavior shown in the plots in Fig. 3 appears to show a drastic decrease, this is only because of the default limits for the signal strength axis (y axis). Rearranging these limits to the nominal values from 0 to 1 reveal that the spectral measurements indicate graybody behavior as the emissivity is nearly spectrally constant (as more clearly seen in the insets in Fig. 3).

Under the assumption made for local thermal equilibrium, by Kirchoff's law, the equivalence of the signal strength and absorptivity was established. Hence, the values of absorptivity in the melting regime were approximated to span from ~0.5 right after the onset of melt scanning (following preheating), reaching minimum values of 0.1692 and 0.1690 at 1064 nm and 1070 nm, respectively. This trend is consistent across the data for the 18 layers measured.

Typical reported values for absorptivity at increasing laser powers that induce keyholing show an increasing trend as power also increases [2,29]; this is the case for PBF-LB/M since during keyholing, laser reflections locally enhance and increase the absorption [39]. More specifically, absorptivity values reported in literature for various materials are typically in the range from 0.5–0.7. For example, Trapp *et al.,* reported in situ absorptivity values for 316 L powder exhibiting an increasing trend in the range from 0.35 to ~0.70 at increasing laser powers [29]. In the work by Brandau *et al.*, a setup involving coaxial multispectral imaging was employed in a PBF-LB/M system in the determination of absorbance of the powder bed for various materials in a spectral range from 350–950 nm [40]. In their results, most powder materials exhibited a monotonic decrease in percent absorbance as wavelength increased, and the specific values for Inconel 718 (50–100μm powder size distribution) were in the vicinity of 0.65 at 950 nm. This result is akin to the measurements performed in the current work for preheated powder (yellow region in Fig. 2), although not the specific focus reported here. Following up, absorptivity values for polished metal substrates and powder samples were presented by Kromer *et al.* [25]. Their technique involved the Ulbricht method using irradiation of samples with a YB:YAG laser (1.03μ m) within an integrating sphere. The powder samples of various thicknesses (50–300μm range) exhibited percent absorptivity values ranging from 0.72 % for Cu to ~65 % for Gr. 5 titanium alloy TA6V under irradiation with a spot size of 2 mm. Their results for irradiation with a spot size of 0.2 mm for 100 ms indicated a decreasing trend during a transition phase (involving sintering after ~1 ms) for both AlSi10Mg and TA6V. The results obtained in the study by Kromer *et al.*, are consistent with the observations seen in the current work showing a decreasing trend of absorptivity as the melting (i.e. increasing temperatures) ensued. Computationally calculated values for the absorptivity of laser light for various materials including 316L were reported by Boley *et al.* in [41]. Their analysis employed ray tracing and a comprehensive absorption model for mono- and multi-size packed spheres forming powder beds under simulated

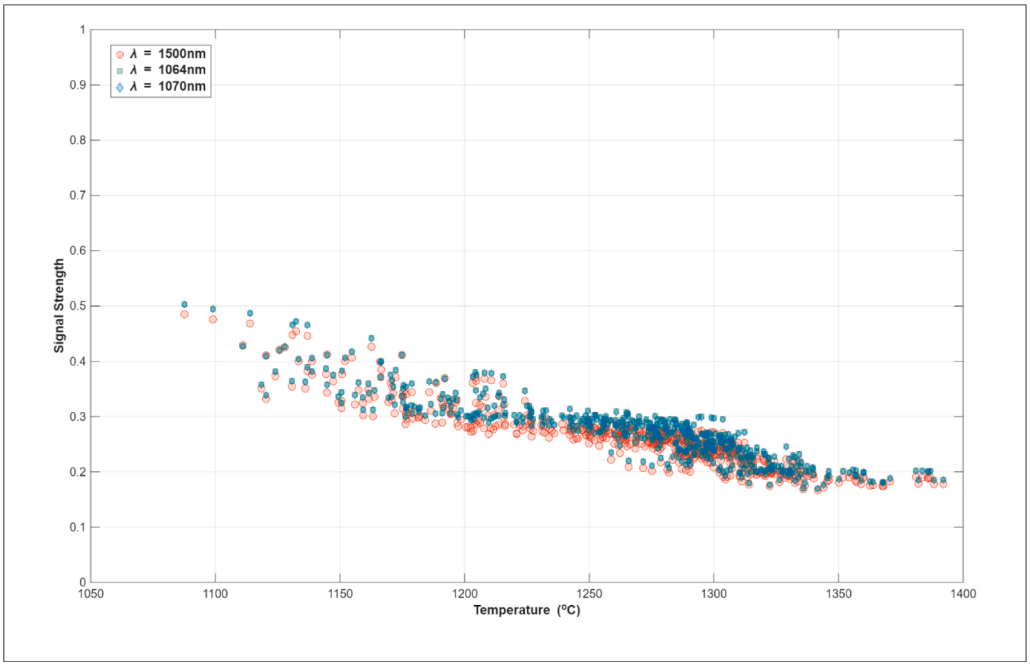

Fig. 4. Signal strength versus temperature during melt scanning for measured (1500 nm, red markers) versus approximated (1064 and 1070 nm, green squares and blue diamonds, respectively). Aggregated data for 18 layers. Markers differentiate wavelengths.

irradiation of a 1μm laser perpendicular to the powder bed. Their study showed that multiple scattering of the laser light enhanced the absorption coefficient for the simulated powder beds. Their absorptivity values for 316L were calculated at ~0.60 for various arrays of simulated particle sizes. Similarly, absorptivity values for various powders were presented by Rubenchik *et al.* from a calorimetry-based experiment using a simple flat-top irradiating beam of 1μ m wavelength [27]. Their results showed a nearly constant absorptivity for Ti6Al4V (~0.7), 316L (~0.6) and AlSi10Mg (~0.5) in the temperature range from 50–500 °C. The study also reported noticeable effects from oxidation at temperatures above 500 °C, suggesting the need for measurements at these and higher temperatures. The study by Li *et al.*, described modeling of several variables for the PBF-LB/M for a titanium alloy, where their model predicted an increase in the absorptivity of the material as power increased [42]. Measurements of absorptivity for Inconel 718 and Inconel 738LC samples were presented by Honda and Watanabe [43] also employing a calorimetric method adapted within a commercial PBF-LB/M system purged in Argon where the samples were irradiated with the system's 1070 nm gaussian laser beam. Their results showed essentially constant values of absorptivity of ~0.6 for both alloys within the temperature range from 150–400 °C.

As can be seen, the values approximated in this work for Inconel 625 show general agreement with values in literature obtained through calorimetry or reflectivity measurements for other powder materials. Particularly for the results presented by [43] for similar nickel-base alloys. Nevertheless, a subtle difference is the fact that the findings presented here indicate that absorptivity decreases to values below 0.2 while in the molten state. This difference is explained by the fact that, compared to the studies surveyed in literature, the results presented in our work are for substantially more elevated temperatures as the measurements originated from the PBF-EB/M process, which is generally carried out with powder beds that are at higher temperatures compared to PBF-LB/M. For example, the data presented by Honda and Watanabe is only for maximum temperatures in the range from ~450–500 °C whereas our data ranges slightly over the melting range of the material at nearly 1400 °C. In the study by Kwon *et al.* using an integrating sphere with irradiation using 1.07μm and 10.6μm laser sources showed a thermal dependence of the absorptivity, up to the melting point for Al, 304 stainless steel and titanium [44]. Their results showed increasing absorptivity, for example from 30 % to about 50 % for 304, but the study did not control the oxidation at elevated temperatures and the samples consisted of polished plates rather than powder, which might also explain the discrepancy with the results presented here.

The absorptivity data presented can support modeling and experimental works aimed at increasing our understanding of PBF AM. For example, a method was recently described to reduce spatter generation during PBF-LB/M in [45]. Spatter, which can indicate non-optimal processing and perhaps the undesired generation of defects [46,47], is generally associated with the scanning conditions and the absorptivity of the laser energy, which changes according to the vectors during scanning. The method in [45], while not directly informed by *in situ* absorptivity values, reduced spatter by controlling the power at the start and end of scanned vectors, effectively compensating for the changing absorption conditions of the laser. In this context, the use of the data we have presented in this work can help to implement similar approaches, informed by in situ absorptivity data, to control scanning conditions and minimize defects in PBF-LB/M.

Conclusion

The data and analysis presented elucidates the behavior or trend of absorptivity at elevated temperatures (over 1000 °C) as the Inconel 625 material transitioned from heated powder to the molten state, which has direct implications for understanding of the material deposition process during PBF. While the absorptivity values approximated here compare with some of the results in the relevant literature, there is also a contrast as our method was capable of measuring this material response directly during scanning conditions whereas most works report only for *ex situ* conditions that not fully represent the fusion process, and for samples that often require careful and extensive preparation. Hence, our technique has the capability to capture in-process measurements, providing a window into the material behavior not available through other means. A further difference is the fact that our results include measurements at much higher temperatures compared to values reported elsewhere since measurements were made on the PBF-EB/M platform. Nevertheless, the study presented here is not completely representative of the conditions observed during the PBF-LB/M process, in which process variables including the inert gas purge and flow, the development of process effects such as the plasma plume, or the development of the keyhole mode cavities –leading to different absorption conditions for the laser energy– need full consideration. The implementation of a similar setup for measurements within a PBF/LB/M system is precisely one of the directions to be pursued as future work.

The results presented in this work are relevant since the data presented can help increase the accuracy of models used for simulation of metal processing methods in AM while also increasing understanding of powder bed fusion processes and leading to the implementation of solutions that can improve and further their commercial application. Our future work also concentrates on these issues; employing data (such as absorptivity) informed approaches to control scanning strategies that improve the processing of metal AM techniques to further the level of trust and utilization of these techniques for various applications.

Declaration of generative AI and AI-assisted technologies in the manuscript preparation process

No AI or AI-assisted technologies were employed for the preparation of this manuscript.

CRediT authorship contribution statement

Shadman Tahsin Nabil: Writing – review & editing, Writing – original draft, Visualization, Validation, Formal analysis, Data curation, Conceptualization. **Alfonso Fernandez:** Writing – review & editing, Software, Methodology, Investigation. **Francisco Medina:** Writing – review & editing, Supervision. **Ralph Felice:** Writing – review & editing, Validation, Formal analysis. **James P. Carney:** Writing – review & editing, Supervision, Funding acquisition. **César A. Terrazas-Nájera:** Writing – review & editing, Writing – original draft, Visualization, Supervision, Methodology, Investigation, Formal analysis, Conceptualization.

Declaration of competing interest

The authors declare that they have no known competing financial interests or personal relationships that could have appeared to influence the work reported in this paper.

Acknowledgements

The research described here was performed at The University of Texas at El Paso (UTEP) within the W.M. Keck Center for 3D Innovation (Keck Center). This material is based on research sponsored by, in part, the Air Force Research Laboratory (AFRL) under agreement number FA8650-20-2-5700. Additional support was provided by strategic investments via discretionary UTEP Keck Center funds and the Mr. and Mrs. MacIntosh Murchison Chair I in Engineering Endowment at UTEP (RWB). The U.S. Government is authorized to reproduce and distribute reprints for Governmental purposes notwithstanding any copyright notation thereon. The views and conclusions contained herein are those of the authors and should not be interpreted as necessarily representing the official policies or endorsements, either expressed or implied, of AFRL or

the U.S. Government.

Data availability

Data will be made available on request.

References

[1] C. Zhao, B. Shi, S. Chen, D. Du, T. Sun, B.J. Simonds, K. Fezzaa, A.D. Rollett, Laser melting modes in metal powder bed fusion additive manufacturing, Rev. Mod. Phys. 94 (2022) 045002, https://doi.org/10.1103/RevModPhys.94.045002.

[2] W.E. King, H.D. Barth, V.M. Castillo, G.F. Gallegos, J.W. Gibbs, D.E. Hahn, C. Kamath, A.M. Rubenchik, Observation of keyhole-mode laser melting in laser powder-bed fusion additive manufacturing, J. Mater. Process. Technol. 214 (2014) 2915–2925, https://doi.org/10.1016/J.JMATPROTEC.2014.06.005.

[3] J.B. Forien, N.P. Calta, P.J. DePond, G.M. Guss, T.T. Roehling, M.J. Matthews, Detecting keyhole pore defects and monitoring process signatures during laser powder bed fusion: a correlation between in situ pyrometry and ex situ X-ray radiography, Addit. Manuf. 35 (2020) 101336, https://doi.org/10.1016/j.addma.2020.101336.

[4] Z. Ren, L. Gao, S.J. Clark, K. Fezzaa, P. Shevchenko, A. Choi, W. Everhart, A. D. Rollett, L. Chen, T. Sun, Machine learning–aided real-time detection of keyhole pore generation in laser powder bed fusion, Science (1979) 379 (2023) 89–94, https://doi.org/10.1126/SCIENCE.ADD4667.

[5] B. Brandau, A. Da Silva, C. Wilsnack, F. Brueckner, A.F.H. Kaplan, Absorbance study of powder conditions for laser additive manufacturing, Mater. Des. 216 (2022) 110591, https://doi.org/10.1016/J.MATDES.2022.110591.

[6] M. Colopi, A.G. Demir, L. Caprio, B. Previtali, Limits and solutions in processing pure Cu via selective laser melting using a high-power single-mode fiber laser, Int. J. Adv. Manufact. Technol. 104 (2019) 2473–2486, https://doi.org/10.1007/S00170-019-04015-3/FIGURES/12.

[7] M. Hummel, C. Schöler, A. Häusler, A. Gillner, R. Poprawe, New approaches on laser micro welding of copper by using a laser beam source with a wavelength of 450 nm, J. Adv. Join. Process. 1 (2020) 100012, https://doi.org/10.1016/J.JAJP.2020.100012.

[8] S. Gruber, L. Stepien, E. López, F. Brueckner, C. Leyens, Physical and geometrical properties of additively manufactured pure copper samples using a green laser source, Mater. (Basel) 14 (2021) 3642, https://doi.org/10.3390/MA14133642.

[9] S.G. Kang, R. Gainov, D. Heußen, S. Bieler, Z. Sun, K. Weinberg, G. Dehm, R. Ramachandramoorthy, Green laser powder bed fusion based fabrication and rate-dependent mechanical properties of copper lattices, Mater. Des. 231 (2023) 112023, https://doi.org/10.1016/J.MATDES.2023.112023.

[10] D. Wang, K. Li, J. Yao, B. Du, Y. Xu, Porosity, texture, and mechanical properties of pure copper fabricated by fine green laser powder bed fusion, Opt. Laser. Technol. 181 (2025) 112009, https://doi.org/10.1016/J.OPTLASTEC.2024.112009.

[11] T. Romano, A. Ratkus, S. Gruber, M. Pozzi, H. Kos, C. Garion, S. Rorison, E. López, T. Torims, M. Vedani, Pure copper membranes manufactured by green laser powder bed fusion with varying wall-thickness and building orientation: microstructure, properties, and vacuum tightness performance, Vacuum 233 (2025) 113995, https://doi.org/10.1016/J.VACUUM.2024.113995.

[12] T.T. Roehling, R. Shi, S.A. Khairallah, J.D. Roehling, G.M. Guss, J.T. McKeown, M. J. Matthews, Controlling grain nucleation and morphology by laser beam shaping in metal additive manufacturing, Mater. Des. 195 (2020) 109071, https://doi.org/10.1016/J.MATDES.2020.109071.

[13] R. Esmaeilzadeh, J. Jhabvala, L. Schlenger, M. van der Meer, E. Boillat, C. Cayron, A.M. Jamili, J. Xiao, R.E. Logé, Toward architected microstructures using advanced laser beam shaping in laser powder bed fusion of Ti-6Al-4V, Adv. Funct. Mater. (2025) 2420427, https://doi.org/10.1002/ADFM.202420427;WGROUP:STRING:PUBLICATION.

[14] F. Galbusera, L. Caprio, B. Previtali, A.G. Demir, The influence of novel beam shapes on melt pool shape and mechanical properties of LPBF produced Al-alloy, J. Manuf. Process. 85 (2023) 1024–1036, https://doi.org/10.1016/J.JMAPRO.2022.12.007.

[15] N. Azizi, E. Jabari, M. Hasanabadi, E. Toyserkani, High-power laser powder bed fusion of Cu–Cr–Zr alloy: a comprehensive study on statistical process optimization, microstructure, and mechanical properties, J. Manuf. Process. 149 (2025) 931–954, https://doi.org/10.1016/J.JMAPRO.2025.06.007.

[16] M. Colopi, L. Caprio, A.G. Demir, B. Previtali, Selective laser melting of pure Cu with a 1 kW single mode fiber laser, Proced. CIRP. 74 (2018) 59–63, https://doi.org/10.1016/J.PROCIR.2018.08.030.

[17] S.D. Jadhav, L.R. Goossens, Y. Kinds, B. Van Hooreweder, K. Vanmeensel, Laser-based powder bed fusion additive manufacturing of pure copper, Addit. Manuf. 42 (2021) 101990, https://doi.org/10.1016/J.ADDMA.2021.101990.

[18] H. Zheng, Y. Wang, Y. Xie, S. Yang, R. Hou, Y. Ge, L. Lang, S. Gong, H. Li, Observation of vapor plume behavior and process stability at single-track and multi-track levels in laser powder bed fusion regime, Metal. (Basel) 11 (2021) 937, https://doi.org/10.3390/MET11060937/S1.

[19] S.A. Khairallah, A.T. Anderson, A. Rubenchik, W.E. King, Laser powder-bed fusion additive manufacturing: physics of complex melt flow and formation mechanisms of pores, spatter, and denudation zones, Acta Mater. 108 (2016) 36–45, https://doi.org/10.1016/J.ACTAMAT.2016.02.014.

[20] A.N.D. Gasper, B. Szost, X. Wang, D. Johns, S. Sharma, A.T. Clare, I.A. Ashcroft, Spatter and oxide formation in laser powder bed fusion of Inconel 718, Addit. Manuf. 24 (2018) 446–456, https://doi.org/10.1016/j.addma.2018.09.032.

[21] M.J. Matthews, G. Guss, S.A. Khairallah, A.M. Rubenchik, P.J. Depond, W.E. King, Denudation of metal powder layers in laser powder bed fusion processes, Acta Mater. 114 (2016) 33–42, https://doi.org/10.1016/j.actamat.2016.05.017.

[22] Z.J. Li, H.L. Dai, J. Xu, Z.W. Huang, A semi-analytical approach for analysis of thermal behaviors coupling heat loss in powder bed fusion, Int. J. Heat. Mass Transf. 201 (2023) 123621, https://doi.org/10.1016/J.IJHEATMASSTRANSFER.2022.123621.

[23] A. Seifter, K. Boboridis, A.W. Obst, Emissivity measurements on metallic surfaces with various degrees of roughness: a comparison of laser polarimetry and integrating sphere reflectometry. Int J Thermophys, Springer, 2004, pp. 547–560, https://doi.org/10.1023/B:IJOT.0000028489.81327.b7.

[24] D.C. Deisenroth, S. Mekhontsev, B. Lane, Measurement of mass loss, absorbed energy, and time-resolved reflected power for laser powder bed fusion, https://doi.org/10.1117/12.2547491 11271 (2020) 46–58. doi:10.1117/12.2547491.

[25] R. Kromer, C. Gorny, E. Gruhier, E. Le Guen, C. Arvieu, E. Lacoste, Absorptivity measurement of solid and powder bed under IR laser beam, Opt. Laser. Technol. 157 (2023) 108508, https://doi.org/10.1016/J.OPTLASTEC.2022.108508.

[26] D. Bergström, J. Powell, A.F.H. Kaplan, The absorptance of steels to Nd:YLF and Nd:YAG laser light at room temperature, Appl. Surf. Sci. 253 (2007) 5017–5028, https://doi.org/10.1016/J.APSUSC.2006.11.018.

[27] M. LeBlanc, A. Rubenchik, S. Mitchell, I. Golosker, N. Peterson, S. Wu, Direct measurements of temperature-dependent laser absorptivity of metal powders, Appl. Opt. 54 (24) (2015) 7230–7233, https://doi.org/10.1364/AO.54.007230.

[28] B.J. Simonds, J. Sowards, J. Hadler, E. Pfeif, B. Wilthan, J. Tanner, C. Harris, P. Williams, J. Lehman, Time-resolved absorptance and melt pool dynamics during intense laser irradiation of a metal, Phys. Rev. Appl. 10 (2018) 044061, https://doi.org/10.1103/PhysRevApplied.10.044061.

[29] J. Trapp, A.M. Rubenchik, G. Guss, M.J. Matthews, In situ absorptivity measurements of metallic powders during laser powder-bed fusion additive manufacturing, Appl. Mater. Today 9 (2017) 341–349, https://doi.org/10.1016/j.apmt.2017.08.006.

[30] B. Lane, I. Zhirnov, S. Mekhontsev, S. Grantham, R. Ricker, S. Rauniyar, K. Chou, Transient laser energy absorption, Co-axial melt pool monitoring, and relationship to melt pool morphology, Addit. Manuf. 36 (2020) 101504, https://doi.org/10.1016/J.ADDMA.2020.101504.

[31] C.A. Terrazas-Nájera, A. Romero, R. Felice, R. Wicker, Multi-wavelength pyrometry as an in situ diagnostic tool in metal additive manufacturing: detecting sintering and liquid phase transitions in electron beam powder bed fusion, Addit. Manuf. (2022). In review.

[32] C.A. Terrazas-Nájera, A. Fernández, R. Felice, R. Wicker, On the thermal emissive behavior of four common alloys processed via powder bed fusion additive manufacturing, Addit. Manuf. 82 (2024) 104023, https://doi.org/10.1016/J.ADDMA.2024.104023.

[33] R.A. Felice, The spectropyrometer – a practical multi-wavelength pyrometer, in: 8th Symposium on Temperature: Its Measurement and Control in Science and Industry, 2002.

[34] R.A. Felice, The spectropyrometer-a practical multi-wavelength pyrometer, n.d. www.pyrometry.com (accessed May 9, 2019).

[35] A. Fernandez, R. Felice, C.A. Terrazas, R. Wicker, Implications for accurate surface temperature monitoring in powder bed fusion: using multi-wavelength pyrometry to characterize spectral emissivity during processing, Addit. Manuf. (2021) 102138, https://doi.org/10.1016/j.addma.2021.102138.

[36] Z.J. Li, H.L. Dai, Y. Yao, J.L. Liu, Energy-based performance prediction for metals in powder bed fusion, Int. J. Mech. Sci. 265 (2024) 108887, https://doi.org/10.1016/J.IJMECSCI.2023.108887.

[37] R.A. Felice, Temperature determining device and process, US 6379,038 B1, 2002.

[38] Y.S. Tolukian, D.P. DeWitt, Thermal radiative properties - metallic elements and alloys, in: Thermophysical Properties of Matter, 1970.

[39] T.R. Allen, W. Huang, J.R. Tanner, W. Tan, J.M. Fraser, B.J. Simonds, Energy-coupling mechanisms revealed through simultaneous keyhole depth and absorptance measurements during laser-metal processing, Phys. Rev. Appl. 13 (2020) 064070, https://doi.org/10.1103/PHYSREVAPPLIED.13.064070/ISICI_SUPPLEMENTARYMATERIAL_PRAPPL.PDF.

[40] B. Brandau, F. Brueckner, A.F.H. Kaplan, Absorbance determination of a powder bed by high resolution coaxial multispectral imaging in laser powder bed fusion, Opt. Laser. Technol. 168 (2024) 109780, https://doi.org/10.1016/J.OPTLASTEC.2023.109780.

[41] S.A. Khairallah, A.M. Rubenchik, C.D. Boley, Calculation of laser absorption by metal powders in additive manufacturing, Appl. Opt. 54 (9) (2015) 2477–2482, https://doi.org/10.1364/AO.54.002477.

[42] Z.J. Li, H.L. Dai, C. Du, P. Xiao, Y. Yao, Energy-based efficient residual stress prediction of titanium alloys with lack-of-fusion porosity in powder bed fusion, Thin-Wall. Struct. 196 (2024) 111513, https://doi.org/10.1016/J.TWS.2023.111513.

[43] H. Honda, M. Watanabe, Measurement of laser absorptivity of inconel powders with additive manufacturing machine, (2024). https://doi.org/10.2320/matertrans.MT-M2024124.

[44] H. Kwon, W.K. Baek, M.S. Kim, W.S. Shin, J.J. Yoh, Temperature-dependent absorptance of painted aluminum, stainless steel 304, and titanium for 1.07 μm and 10.6 μm laser beams, Opt. Lasers. Eng. 50 (2012) 114–121, https://doi.org/10.1016/J.OPTLASENG.2011.10.001.

[45] H.C. Taylor, R.B. Wicker, Impacts of microsecond control in laser powder bed fusion processing, Addit. Manuf. 60 (2022) 103239, https://doi.org/10.1016/J.ADDMA.2022.103239.
[46] N. Bonato, F. Zanini, S. Carmignato, Prediction of spatter-related defects in metal laser powder bed fusion by analytical and machine learning modelling applied to off-axis long-exposure monitoring, Addit. Manuf. 94 (2024) 104504, https://doi.org/10.1016/J.ADDMA.2024.104504.
[47] T.T. Ikeshoji, M. Yonehara, C. Kato, Y. Yanaga, K. Takeshita, H. Kyogoku, Spattering mechanism of laser powder bed fusion additive manufacturing on heterogeneous surfaces, Sci. Rep. 12 (2022) 1–13, https://doi.org/10.1038/S41598-022-24828-9;SUBJMETA.